A bedform phase diagram for dense granular currents

[1]Gregory Smith*, [1]Peter Rowley, [1]Rebecca Williams, [2]Guido Giordano, [2]Matteo Trolese, [2]Aurora Silleni, [3]Daniel R. Parsons, [4]Samuel Capon

[1]*Department of Geography, Geology and Environment, University of Hull, Hull, UK*

[2]*Dipartimento di Scienze, Università Roma Tre, Roma, Italia*

[3]*Energy and Environment Institute, University of Hull, Hull, UK*

[4]*School of Earth and Environmental Sciences, University of Portsmouth, Portsmouth, UK*

**Gregory.Smith@2016.hull.ac.uk*

This paper is a non-peer reviewed preprint submitted to EarthArXiv.

A bedform phase diagram for dense granular currents

Pyroclastic density currents are a life-threatening volcanic hazard. Our understanding and hazard assessments of these flows primarily rely on interpretations of their deposits. The occurrence of stratified layers, cross-stratification, and dune bedforms in these deposits has been assumed as indicative of dilute, turbulent, flows causing traction-dominated deposition. Here we show, through analogue experiments, that a variety of dune bedforms can be produced by denser, aerated, granular currents, including regressive dune bedforms that are formed in waning flows by an upstream-propagating granular bore. We are able to, for the first time, define phase fields for the formation of dune bedforms in PDC deposits. We examine how our findings impact the understanding of bedform features in outcrop, using the example of the Pozzolane Rosse ignimbrite of the Colli Albani volcano, Italy, and thus highlight that interpretations of the formative mechanisms of these features observed in the field must be reconsidered.

INTRODUCTION

Particulate density currents are the biggest mass transporters of sediment on the Earth's surface. Deep sea turbidity currents form the largest sediment accumulations on Earth[1], density currents emplace ejecta blankets around bolide impact craters[2] and individual pyroclastic density currents (PDCs) can transport thousands of cubic kilometers of volcanic material[3]. These flows also pose a major geohazard, with turbidity currents threatening seafloor infrastructure and PDCs being responsible for over 90,000 deaths since 1600AD[4,5]. Understanding the behaviour of these particle-laden, fast-moving currents is fundamental to decreasing the risks they pose to society.

The dynamics and depositional processes of PDCs are difficult to analyse due to a PDCs destructiveness, and the concealment of the interior dynamics by an accompanying ash cloud. Understanding of PDC behaviour therefore, is primarily based on analogue and numerical modelling[6-9], and interpretation of the geological record preserved in sedimentary deposits[10-14].

Analogue modelling of dense PDCs has advanced considerably over recent years including work focusing on the influence of pore pressure[8,15-20]. High gas pore pressures created by various mechanisms within PDCs[10,13,21-23] has been shown to be responsible for their unusually high mobility[24-26], but only recently has physical modelling reflected the sustained and variable nature of such pore pressures with distance from source[19,27].

The presence and morphology of sedimentary structures, such as dune bedforms, in a deposit can be interpreted to tell us about the internal behaviour of the density current that formed them[28-32]. Various dune bedforms occur in PDC-generated ignimbrites and are assumed to be formed as deposits from dilute, high-velocity (surge), PDCs[12,31,33-35], where tractional processes dominate in the flow-boundary zone due to the predominance of fluid turbulence as a particle support mechanism[6,13,36,37]. Denser, granular-fluid based, PDCs are usually thought to be responsible for creation of massive deposits, lacking in sedimentary structures[10,13,38,39].

Dune bedforms in PDC deposits include structures whose morphologies have drawn comparisons with fluvial chute-and-pool structures and antidunes (Fig. 1a & 1f and Fig. 1b & 1d), which are formed under supercritical hydraulic flow conditions[29,32,40,41]. The widespread interpretation of such structures in PDC deposits is that they are also the result of supercritical flow[12,33,42-45].

Recently, however, there have been attempts to introduce new terminology, which does not hold the genetic connotations of ‘antidune’ or ‘chute-and-pool’. Douillet et al.[35] introduce the term ‘regressive climbing dunes’ for dune bedforms which show upstream crest migration (Fig. 1c). Brand et al.[46] adopt similar terminology, using ‘progressive dune bedforms’ and ‘regressive dune bedforms’ (Fig. 1e). In this paper we follow Brand et al.[46] in using the term ‘regressive dune bedform’ to describe upstream-migrating dune bedforms which have both asymmetrical (much steeper stoss sides) (Fig. 1g) or roughly symmetrical lee and stoss slopes (Fig. 1h).

Here we examine, for the first time, the conditions which promote the growth of dune bedforms in aerated dense granular flows, as analogues for PDCs and their deposits. The present work describes laboratory experiments in which use partially fluidised (“aerated”) fine-grained ballotini sediment in a 3 m long flume (see Methods). These experiments are able to simulate many behaviours of PDCs[8,18,19,27]. As deposition aggrades from the quasi-steady currents, the growth of dune bedforms is recorded using high speed video. We study how dune bedform features form within the dense granular currents as a result of rapid deposition and the propagation of a granular bore. We are able to, for the first time, define phase fields for the formation of dune bedforms in ignimbrites using current velocity, current thickness, Froude number, and Friction number. We examine how our interpretations impact on the understanding of similar features in outcrop, using the example of the Pozzolane Rosse ignimbrite of the Colli Albani volcano, Italy.

RESULTS

Dune Bedform morphology

A range of bedforms were observed growing under a variety of flow conditions within the suite of experimental runs (see Methods). We categorise these bedforms into three types (Fig. 2): i) planar/very shallowly dipping (<2°) regressive beds, ii) regressive dune bedforms with shallow stoss sides less than the dynamic angle of repose ($< \Theta_{Dyn}$), and iii) regressive dune bedforms with steep ($>\Theta_{Dyn}$) stoss sides.

Where steep regressive dune bedforms are present, they comprise multiple (3-4) stoss-side packages dipping at varying angles, and a single corresponding lee-side bed. Dune bedform lengths and thicknesses are reported, as opposed to wavelengths and amplitudes, as we do not produce repetitive trains of bedforms. When reporting the length of a dune bedform, the distance from the onset of the stoss-side packages to the termination of the lee slope on the depositional surface is measured (similar to a half-wavelength). Thickness refers to the maximum thickness of the entire dune bedform, perpendicular to its base (Fig. 1g and 1h).

Shallow regressive dune bedforms have form lengths between 0.18 m and 0.21 m and thicknesses between 0.003 m and 0.01 m. Stoss and lee sides have similar dip angles (90 % below 10°, see Fig. 8d), and successive crests migrate upstream, forming aggrading cross-beds (Fig. 2).

Steep regressive dune bedforms have form lengths between 0.4 m and 0.18 m and thicknesses between 0.35 m and 0.4 m. Stoss sides are considerably steeper (>20°) than lee sides (< 10°, Fig. 8d), and each stoss-side package has a roughly sigmoidal shape. These also aggrade upstream, with stoss angles becoming progressively steeper (20°-90°) (Fig. 2a-d).

Dune Bedform deposition

The leading edges of the currents were travelling at ~2 ms^{-1} as they passed into the lesser/un-aerated second chamber of the flume (Fig. 3a, see Supplementary Video 1). The sustained, quasi-steady body of the currents are slowed by the more rapid deaeration as they enter the second chamber, and deposition begins. The currents, with velocities of ~1-1.5 ms^{-1}, initially deposit planar or very shallow upstream-dipping beds (Fig. 3b). As the current velocity further decreases and deposit thickness increases, upstream-migrating shallow dune bedforms are deposited, their stoss sides forming shallow regressive beds (Fig. 3c-d). At lower velocities still (below ~ 0.5 ms^{-1}), the upstream edge of the deposit steepens and collapses, with very steep regressive beds deposited just prior to this, forming the stoss sides of steep regressive dune bedforms (Fig. 3e-f).

Velocity and thickness control on bedform formation

Current velocities and thicknesses during deposition of the dune bedforms were measured (Supplementary Table 1) and plotted (Fig. 4a). Error for current thickness was calculated at ± 0.0013 m (2σ). Error for current velocity was calculated at ± 0.055 ms^{-1} (2σ). Planar, shallow, and steep features fall into well-defined fields, suggesting that current velocity and thickness controls the sedimentary structures in the deposit. For a given current thickness steep regressive dune bedforms are deposited at lower velocities (between 0.3-0.6 ms^{-1} in these experiments). Shallow regressive dune bedforms are deposited at greater velocities, and planar bedforms are deposited at the highest velocities (above 1 ms^{-1} in these experiments). With increasing current thickness higher current velocities are required to remain in the shallow bedform and planar bedform stability fields. As a result thickening, a steady current can lead to a change in bedform character without a requirement for a change in flow velocity.

Dimensionless parameters

We define phase fields for the three dune bedforms using the Froude number (Fr) and the Friction Number (N_F). The Froude number represents the ratio of kinetic to potential energy (Eq 1).

$$Fr = U/(gH)^{1/2} \qquad \text{(Eq 1)}$$

Where $U = current\ velocity$, $g = gravity$, and $H = current\ thickness$. N_F is the ratio of frictional to viscous stresses and is defined as Bagnold Number/Savage Number. The Savage number (N_S, Eq. 2) is the ratio of collisional stress to frictional stress[47,48], and the Bagnold number (N_B, Eq. 3) is the ratio of collisional stress to viscous fluid stress[48,49].

$$N_S = \frac{\rho_s\left(\frac{U}{H}\right)^2\delta^2}{(\rho_s - \rho_f)gH\tan\theta} \qquad \text{(Eq 2)}$$

$$N_B = \varphi_f - \frac{\rho_s\delta^2\left(\frac{U}{H}\right)}{(1-\varphi_f)\mu} \qquad \text{(Eq 3)}$$

where ρ_s = particle density ρ_f = fluid density δ = particle diameter θ = internal friction angle φ_f = solid volume fraction μ = fluid viscosity.

Froude numbers were calculated for each tracked sediment packages during deposition (±0.17, 2σ). Figure 4a shows how different dune bedforms are formed under different ranges of *Fr*, with greater overlap between the steep and shallow regressive dune bedform fields than between the shallow regressive dune bedform and planar bed fields. Figure 4c shows a good correlation (R = 0.843) between *Fr* and velocity, with a noticeably greater data spread at higher (>0.8 ms^{-1}) velocities, whereas *H* exerts much less of a control on *Fr* (Fig. 4b). Figure 4d plots *Fr* against N_F (±67,000, 2σ). Steep regressive dune bedforms are mostly deposited at *Fr* between 0.9 and 1.4, and N_F between 1×10^5 and 4×10^5. Shallow regressive dune bedforms are mostly deposited at *Fr* between 1.9 and 3.5, and N_F between 3×10^4 and 1.2×10^5. Planar beds are mostly deposited at *Fr* between 3.6 and 6, and N_F between 1×10^4 and 5×10^4.

The planar-shallow-steep sequence of the dune bedform formation records the transition of a fast, supercritical current dominated by viscous stresses to a slower, subcritical current increasingly dominated by frictional stresses.

Field Analogue

The Pozzolane Rosse ignimbrite is an example of where steep regressive bedforms have been deposited by a PDC that is interpreted to be a dense flow (e.g. matrix-supported, fines depleted; Fig. 5). The Pozzolane Rosse covers an area of more than 1600 km^2 around the Colli Albani volcano, Italy[50], and has been dated ($^{40}Ar/^{39}Ar$) at 456 ± 3 ka[51]. It surmounts topography of 250 m to reach altitudes of 440 m[52]. The ignimbrite is generally massive, matrix-supported and poorly-sorted, with a noticeable depletion in fine ash, and in places partially lithified by zeolites[52]. Emplacement temperatures have been calculated to be between 630 °C and 710 °C[53]. Grain size analysis on six representative samples taken from Pozzolane Rosse show they are dominated by lapilli-sized grains and severely depleted in the < 63 µm fraction (Fig. 5). Figure 6 shows that our Pozzolane Rosse samples fall into the ‘Fines-depleted flow’ field of Walker[35], similar to previous work on the ignimbrite[50]. Grains are dominantly poorly vesicular scoria with compositions plotting in the tephrite/basanite field[54]. Rotating drum tests on the six samples taken from the Pozzolane Rosse (excluding grains > 0.0056 m) gave static minimum (Θ_{Smin}), maximum (Θ_{Smax}) and dynamic (Θ_{Dyn}) angles of repose of 35.3°, 51.7° and 45.2° respectively (Supplementary Fig. 1). These values are considerably higher than those obtained for the ballotini used in the experiments (Supplementary Fig. 2), likely due to the variable grainsize, angularity and cohesion of the ignimbrite grains.

The Pozzolane Rosse shares many characteristics with massive ignimbrites which are ubiquitously interpreted as deposits of dense, granular fluid PDCs, with the clear exception of the paradoxical presence of dune bedforms within the deposit, which are typically indicative of dilute, turbulent flow (“pyroclastic surges”). As other indicators of this type of flow, such as well developed, thin stratification, good sorting, and abundance of fines are lacking, we interpret the Pozzolane Rosse to have been deposited by a dense, granular PDC.

Dune bedforms are found in the NE sector of the ignimbrite where it leaves the radial plain and runs up into the Apennine mountains[55]. Figure 7a- c shows some of these dune bedforms and the angles of their stoss sides, several of which are greater than 20°, similar to the stoss angles of our experimental steep dune bedforms (Fig. 7d). Shallow stoss-sided dune bedforms are found in the Pozzolane Rosse, although they tend to have greater lee (due to the greater repose angles of the material) and stoss angles than experimental examples, where both are <10°.

DISCUSSION

Our experimental currents show rapidly evolving Froude numbers. Within the current body, planar beds are deposited at *Fr* 3-5, shallow regressive dune bedforms at *Fr* 2-3, and steep regressive dune bedforms at *Fr* 0.59-2. We show that an apparent hydraulic jump within the flow forms in the current as the deposit thickens (Fig. 8). As the experimental current is granular, we adopt the term granular jump[56-58], which shares many characteristics with its fluvial counterpart. Although the current has a lower *Fr* immediately after the jump than the incoming current, this is not always <1.

The deposition of steep regressive dune bedforms in more conventional hydraulic systems (e.g. alluvial channels or turbidity currents) is related to the formation and propagation of hydraulic jumps, where flow transforms from Froude supercritical (>1) to Froude subcritical (<1). Using this hydraulic model, the existing interpretation of features in PDC deposits, which are visually similar to fluvial chute-and-pool structures[33,34,42,43,46] (Fig. 1a/1e and 1f), is as the product of Froude supercritical flow in dilute PDCs[33,38,42,43,46,59-61]. We have demonstrated that this interpretation can be incorrect, and that similar features can form in dense granular flows in both Froude subcritical and supercritical conditions.

As the sediment deposit which triggered the jump grows in thickness, a critical point is reached where the incoming flow cannot surpass the negative slope, and the jump propagates upstream as a granular bore[57]. An interesting feature seen in the granular jump of Boudet et al.[56] and our own currents is the steepening well beyond the repose angle at the front of the granular jump/bore, and its collapse by avalanching (Fig. 8d). This is likely caused by rapid deposition from the incoming flow countering the effects of gravity sliding, and allowing the bedforms to steepen well beyond repose angle. The particles deposited by the current as the deposit front steepens form our steep regressive dune bedforms, with stoss angles up to 90°.

Calculated N_S and N_B numbers indicate that planar beds are deposited under conditions closer to a collision-dominated flow regime ($N_S > 0.1$ and $N_B > 540$[62]) than the regressive dune bedforms (Supplementary Table 1). The planar bed deposition occurs beyond the transition to the unfluidised section of flume, and therefore they are deposited by a current which is experiencing more collisions between particles due to the loss of gas pore pressure. The regressive dune bedforms are deposited closer to this transition point, where the current has a higher gas pore pressure and grain collisions are not as prevalent. A ratio of N_B to N_S shows that frictional stresses are considerably higher than viscous shear stresses in the area of the currents depositing steep regressive dune bedforms (Fig. 4d). As the current is waning at this point and relatively thick, this could result in sustained contacts between particles despite relatively high gas pore pressures.

The occurrence of dune bedforms in the Pozzolane Rosse ignimbrite supports the experimental supposition that dune bedforms within PDC deposits, hitherto interpreted as been laid down by dilute turbulent PDCs, can be formed by dense granular currents undergoing rapid sedimentation and deceleration. In our experiments, the cessation of basal gas injection and the resulting decrease in pore pressure results in rapid sedimentation; and the steep stoss-sided dune bedforms are created in a waning flow regime. Giordano &

Doronzo[55] interpret the parent PDC in this sector as waning, experiencing rapid sedimentation and a reduction in the lateral mass discharge rate.

We propose a depositional model whereby symmetrical, upstream migrating dune bedforms are deposited by supercritical flow, forming a topographic irregularity which drastically slows the incoming current (Fig. 9a-b), forming a granular jump and promoting rapid deposition (Fig. 9c). Continued deposition steepens the front of the jump until it collapses upstream by avalanching (Fig. 9d-e).

The triggering of initial deposition in the experiments is related to the transition of the current into a non-aerated (or significantly less aerated) chamber of the flume, and the consequent increase in frictional forces between particles. This is not intended to represent a specific natural process but rather simulate the rapid de-aeration we know can occur in natural PDCs as a result of various processes such as loss of fines or temperature drops, thinning, and/or the entrainment of courser material[20,23,63]. The initial de-aeration would be accelerated by the slowing current (decreasing shear rates), and increasing inter-particle frictional forces. The formation of a granular jump within the depositing current is related to the blocking of the flow by the aggrading deposit; a process that could be exacerbated by pre-existing topography[58].

Deposition from our experimental granular currents is triggered by rapid defluidisation, and results in the formation of sedimentary structures which we class (in order of reducing velocity) as: planar beds, shallow regressive dune bedforms, and steep regressive dune bedforms, each of which can be categorised by dune bedform phase diagrams.

We find that the steep regressive dune bedforms are recording the upstream migration of a granular bore, which is caused by interaction of the current with aggrading deposit. The waning nature of the incoming flow at this point, and its relatively low Froude numbers suggests that while most of these steep regressive dune bedforms are technically recording supercritical flow, both the shallow regressive dune bedforms and planar beds are formed under increasingly supercritical conditions. It follows that shallow regressive dune bedforms and planar beds may then be better indicators of supercritical flow conditions when interpreting dense PDC deposits. The proposed phase diagrams presented here are a major step towards quantitative links between PDC processes and their deposits.

Dune bedforms can be the product of a dense granular flow and can form without any interference (e.g. tractional shear) from an overlying dilute turbulent layer. As the presence of dune bedforms has been commonly used as diagnostic evidence for dilute, turbulent currents, our findings have important implications for field interpretation – as different types of PDCs can react differently to topography the correct classification is necessary for hazard assessment. Other sedimentary characteristics such as grain size and sorting must be used in order to distinguish between the two PDC end-members. This challenge to the interpretation of the deposits of particulate granular currents is particularly relevant to other free-surface granular mass flows, including landslides, snow avalanches, and debris flows.

METHODS

Flume set-up

We use the experimental flume of Smith et al.[27], modified so that release of the particulate density current is controlled by a trapdoor instead of a horizontal lock gate (Fig. 10), such that colour stratification in the starting charge transmits to the flow and deposit. The base of the flume comprises one-meter long sections which can provide independently controlled gas fluxes through a porous baseplate in each section in order to fluidise any overpassing material. The flume was kept at an angle of 2°, to promote flow away from the impingement surface while maintaining a sub-horizontal surface.

The air-supply plumbing allows a gas flux to be fed through the base of the flume, producing sustained aeration of the current. In such thin (<0.03 m), rapidly degassing laboratory currents, this enables us to simulate the long-lived high gas pore pressures that characterize thicker PDCs [19,27]. The gas flux supplied through the base in each of the three sections of the channel was controlled to vary the aeration state of the currents, all of which were below minimum fluidisation velocity (U_{mf}), as complete fluidisation would result in non-deposition[18].

Various aeration states were used to trigger different flow behaviours. The first chamber (0.66-0.93 U_{mf}) always had higher gas flux than the second chamber (0-0.66 U_{mf}) to trigger deposition in the target area of the flume. The experiments were recorded using high-speed video at 200 frames per second. This video recorded a side-wall area of the channel at 1 m runout (across the contact between the first and second gas supply chambers), allowing for measurement of the flow conditions.

Experimental material

The experiments were performed using spherical soda lime ballotini with grain sizes of 45-90 μm (average D_{32} = 63.4 μm calculated from six samples across the material batch) similar to the particles used in previous experimental granular currents[15,17,19]. These ballotini belong to the Group A classification of Geldart[64], comprising particles 45-90 μm which expand homogenously above U_{mf} until bubbles form. As PDCs contain dominantly Group A particles, this allows dynamic similarity between the natural and experimental currents[8]. Detailed mechanical properties of the ballotini are presented in Supplementary Table 2, derived from rotating drum[65] and shearbox (BS 1377-7:1990) testing. These give cohesion values of 0 kPa, and an internal friction angle of 25.3° (Supplementary Fig. 3). Static minimum (Θ_{Smin}), maximum (Θ_{Smax}) and dynamic (Θ_{Dyn}) angles of repose are found to be of 11.7°, 31.9° and 20.9° respectively (Supplementary Fig. 2).

Due to the monodisperse nature of the materials, any internal structure is easily masked by lack of contrast between packages of sediment[66]. To this end the charge for each experiment was built up of layers of dyed beads so that flow packages could be tracked throughout flow and deposition, as used in Rowley et al.[19].

REFERENCES

1: Bouma, A. H., Normark, W. R. & Barnes, N. E. Submarine Fans and Related Turbidite Systems. *Frontiers in Sedimentary Geology* (Springer, New York, NY, 1985).

2: Siegert, S., Branney, M. J. & Hecht, L. Density current origin of a melt-bearing impact ejecta blanket. *Geology* **45,** 855-858 (2017).

3: Self, S. The effects and consequences of very large explosive volcanic eruptions. *Philos. T. R. Soc. A* **364** (2006).

4: Auker, M. R., Sparks, R. S. J., Siebert, L., Crossweller, H. S. & Ewert, J. A statistical analysis of the global historical volcanic fatalities record. *J. Appl. Volcanol*. **2** (2013).

5: Tanguy, J.-C., Ribière, Ch., Scarth, A. & Tjetjep, W. Victims from volcanic eruptions: a revised database. *Bull. Volcanol.* **60,** 137-144 (1998).

6: Valentine, G. A. Stratified flow in pyroclastic surges. *Bull. Volcanol.* **49,** 616-630 (1987).

7: Dobran, F., Neri, A. & Macedonio, G. Numerical simulation of collapsing volcanic columns. *J. Geophys. Res.* **98,** 4231-4259 (1993).

8: Roche, O. Depositional processes and gas pore pressure in pyroclastic flows: An experimental perspective. *Bull. Volcanol.* **74,** 1807–1820 (2012).

9: Dufek, J. The fluid mechanics of pyroclastic density currents. *Annu. Rev. Fluid. Mech.* **48,** 459-485 (2016).

10: Sparks, R. S. J. Grain size variations in ignimbrites and implications for the transport of pyroclastic flows. *Sedimentology* **23,** 147–188 (1976).

11: Wilson, C. J. N. The Taupo eruption, New Zealand: II. The Taupo Ignimbrite. *Philos. T. R. Soc. A* **314,** 229-310 (1985).

12: Cas, R. A. F. & Wright, J. V. Volcanic Successions: Modern and Ancient (Allen and Unwin, London, 1987).

13: Branney, M. J. & Kokelaar, P. Pyroclastic density currents and the sedimentation of ignimbrites. *Geol. Soc. London. Memoir* **27** (2002).

14: Pollock, N. M., Brand, B. D., Rowley, P. J., Sarocchi, D., Sulpizio, R. Inferring pyroclastic density current flow conditions using syn-depositional sedimentary structures. *Bull. Volcanol.* (In press, 2019).

15: Roche, O., Gilbertson, M. A., Phillips, J. C. & Sparks, R. S. J. Experimental study of gas-fluidized granular flows with implications for pyroclastic flow emplacement. *J. Geophys. Res.-Sol. Ea.* **109,** B10201 (2004).

16: Girolami, L., Roche, O., Druitt, T. & Corpetti, T. Particle velocity fields and depositional processes in laboratory ash flows, with implications for the sedimentation of dense pyroclastic flows. *Bull. Volcanol.* **72,** 747-759 (2010).

17: Montserrat, S., Tamburrino, A., Roche, O. & Niño, Y. Pore fluid pressure diffusion in defluidizing granular columns. *J. Geophys. Res.* **117,** F02034 (2012).

18: Chédeville, C. & Roche, O. Autofluidization of pyroclastic flows propagating on rough substrates as shown by laboratory experiments. *J. Geophys. Res.-Sol. Ea.* **119,** 1764–1776 (2014).

19: Rowley, P. J., Roche, O., Druitt, T. H. & Cas, R. Experimental study of dense pyroclastic density currents using sustained, gas-fluidized granular flows. *Bull. Volcanol.* **76,** 855 (2014).

20: Gueugneau, V., Kelfoun, K., Roche, O. & Chupin, L. Effects of pore pressure in pyroclastic flows: Numerical simulation and experimental validation. *Geophys. Res. Lett.* **44,** 2194-2202 (2017).

21: Wilson, C. J. N. The role of fluidization in the emplacement of pyroclastic flows: An experimental approach. *J. Volcano. Geotherm. Res.* **8,** 231–249 (1980).

22: Giordano, G. The effect of paleotopography on lithic distribution and facies associations of small volume ignimbrites: the WTT Cupa (Roccamonfina volcano, Italy). *J. Volcanol. Geoth. Res.* **87,** 255-273 (1998).

23: Druitt, T. H., Avard, G., Bruni, G., Lettieri, P. & Maez, F. Gas retention in fine-grained pyroclastic flow materials at high temperatures. *Bull. Volcanol.* **69,** 881–901 (2007).

24: Hayashi, J. & Self, S. A comparison of pyroclastic flow and debris avalanche mobility. *J. Geophys. Res.* **97,** 9063-9071 (1992).

25: Calder, E. et al. Mobility of pyroclastic flows and surges at the Soufriere Hills Volcano, Montserrat. *Geophys. Res. Lett.* **26,** 534-540 (1999).

26: Lube, G. et al. Generation of air lubrication within pyroclastic density currents. *Nat. Geosci.* **12,** 381-386 (2019).

27: Smith, G., Williams, R., Rowley, P. & Parsons, D. Investigation of variable aeration of monodisperse mixtures: implications for pyroclastic density currents. *Bull. Volcanol.* **80,**67 (2018).

28: Bouma, A. H. *Sedimentology of Some Flysch Deposits* (Elsevier, Amsterdam, 1962).

29: Jopling, A. V. & Richardson, E. V. Backset bedding developed in shooting flow in laboratory experiments. *J. Sed. Petrol.* **36,** 821-825 (1966).

30: Normark, W. R., Hess, G. R., Stow, D. A. V. & Bowen, A. J. Sediment waves on the Monterey Fan levee: A preliminary physical interpretation. *Mar. Geol.* **37,** 1-18 (1980).

31: Allen, J. *Sedimentary Structures: Their Character and Physical Basis, Volume 2*. Elsevier, Amsterdam, 1982).

32: Alexander, J., Bridge, J. S., Cheel, R. J. & Leclair, S. F. Bedforms and associated sedimentary structures formed under water flows over aggrading sand beds. *Sedimentology* **48,** 133-152 (2001).

33: Schmincke, H.-U., Fisher, R. V. & Waters, A. C. Antidune and chute and pool structures in the base surge deposits of the Laacher See area, Germany. *Sedimentology* **20,** 553-574 (1973).

34: Cole, P. Migration direction of sand-wave structures in pyroclastic-surge deposits: implications for depositional processes. *Geology* **19,** 1108-1111 (1991)

35: Douillet, G. A. et al. Dune bedforms produced by dilute pyroclastic density currents from the August 2006 eruption of Tungurahua volcano, Ecuador. *Bull. Volcanol.* **75,** 762 (2013).

36: Walker, G. P. L. Ignimbrite types and ignimbrite problems. *J. Volcano. Geotherm. Res.* **17,** 65-88 (1983).

37: Dellino, P., Mele, D., Sulpizio, R., La Volpe, L. & Braia, G. A method for the calculation of the impact parameters of dilute pyroclastic density currents based on deposit particle characteristics. *J. Geophys. Res.* **113,** B07206 (2008).

38: Fisher, R. V., Schmincke, H-.U. & Van Bogaard, P. Origin and emplacement of a pyroclastic flow and surge unit at Laacher See, Germany. *J. Volcanol. Geotherm. Res.* **17,** 375-392 (1983).

39: Cas, R. A. F. et al. The flow dynamics of an extremely large volume pyroclastic flow, the 2.08-Ma Cerro Galán ignimbrite, NW Argentina, and comparison with other flow types. *Bull. Volcanol.* **73,** 1583-1609 (2011).

40: Middleton, G. V. Antidune cross-bedding in a large flume. *J. Sed. Petrol.* **35,** 922-927 (1965).

41: Cartigny, M. J. B., Ventra, D., Postma, G. &Van Den Berg, J. H. Morphodynamics and sedimentary structures of bedforms under supercritical-flow conditions: New insights from flume experiments. *Sedimentology* **21,** 712-748 (2014).

42: Fisher, R. & Waters, A. Bed forms in Base-Surge deposits: Lunar implications. *Science* **26,** 1349-1352 (1969).

43: Fisher, R. & Waters, A. Base surge bed forms in maar volcanoes. *Am. J. Sci.* **268,** 157-180 (1970).

44: Waters, A. C. & Fisher, R. V. Base surges and their deposits: Capelinhos and Taal volcanoes. *J. Geophys. Res.* **76,** 5596–5614 (1971).

45: Crowe, B. & Fisher, R. Sedimentary structures in base-surge deposits with special reference to cross-bedding, ubehebe craters, death valley, California. *Bull. Geol. Soc. Am.* **84,** 663-682 (1973).

46: Brand, B., Bendaña, S., Self, S. & Pollock, N. Topographic controls on pyroclastic density current dynamics: Insight from 18 May 1980 deposits at Mount St. Helens, Washington (USA). *J. Volcano. Geotherm. Res.* **321,** 1-17 (2016).

47: Savage, S. B. & Hutter, K. The motion of a finite mass of granular material down a rough incline. *J. Fluid Mech.* **199,** 177-215 (1989).

48: Iverson, R. M. The physic of debris flows. *Rev. Geophys*. **35,** 245-296 (1997).

49: Bagnold, R. A. Experiments on a gravity-free dispersion of large solid spheres in a Newtonian fluid under shear. *Proc. R. Soc. London, Ser. A* **225,** 49-63 (1954).

50: Giordano, G. & Dobran, F. Computer simulations of the Tuscolano Artemisio's second pyroclastic flow unit (Alban Hills, Latium, Italy). *J. Volcanol. Geoth. Res.* **61,** 69-94 (1994).

51: Marra, F., Karner, D. B., Freda, C., Gaeta, M. & Renne, P. Large mafic eruptions at Alban Hills Volcanic District (Central Italy): Chronostratigraphy, petrography and eruptive behavior. *J. Volcanol. Geotherm. Res.* **179,** 217–232 (2009).

52: Giordano, G. et al. Stratigraphy, volcano tectonics and evolution of the Colli Albani volcanic field. In: Funiciello, R., Giordano, G. (Eds.) *The Colli Albani Volcano Spec. Publ. IAVCEI* **3,** 43-98 (2010).

53: Trolese, M., Giordano, G., Cifelli, F., Winkler, A. & Mattei, M. Forced transport of thermal energy in magmatic and phreatomagmatic large volume ignimbrites: Paleomagnetic evidence from the Colli Albani volcano, Italy. *Earth. Planet. Sc. Lett.* **478,** 179-191 (2017).

54: Conticelli, S. et al. (2010) Geochemistry, isotopes and mineral chemistry of the Colli Albani volcanic rocks: constraints on magma genesis and evolution. In: Funiciello, R., Giordano, G. (Eds.) *The Colli Albani Volcano, Spec. Publ. IAVCEI* **3,** 107-139 (2010).

55: Giordano, G. & Doronzo, D. M. Sedimentation and mobility of PDCs: a reappraisal of ignimbrites' aspect ratio. *Sci. Rep.* **7,** 1-7 (2017).

56: Boudet, J. F., Amarouchene, Y., Bonnier, B. & Kellay, H. The granular jump. *J. Fluid. Mech.* **572,** 413-431 (2007).

57: Faug, T. Depth-averaged analytic solutions for free-surface granular flows impacting rigid walls down inclines. *Phys. Rev. E* **92,** 062310 (2015).

58: Faug, T., Childs, P., Wyburn, E. & Einav, I. Standing jumps in shallow granular flows down smooth inclines. *Phys. Fluids.* **27,** 073304 (2015).

59: Wohletz, K. H. & Sheridan, M. F. A model of pyroclastic surge. *Geol. Soc. Am. Sp. Pap.* **180,** 177–194 (1979).

60: Sohn, Y. K. & Chough, S. K. Depositional processes of the Suwolbong tuff ring, Cheju Island (Korea). *Sedimentology* **36,** 837-855 (1989).

61: Gençalioğlu-Kuşcu, C., Atilla, C., Cas, R. A. F. & Kuşcu, I. Base surge deposits, eruption history, and depositional processes of a wet phreatomagmatic volcano in Central Anatolia (Cora Maar). *J. Volcano. Geotherm. Res.* **159,** 198-209 (2007).

62: Iverson, R. M. & Denlinger, R. P. Flow of variably fluidized granular masses across three-dimensional terrain: 1. Coulomb mixture theory. *J. Geophys. Res.* **106,** 537-552 (2001).

63: Bareschino, P. et al. Fluidization and de-aeration of pyroclastic mixtures: the influence of fines content, polydispersity and shear flow. *J. Volcanol. Geotherm. Res.* **164,** 284–292 (2007).

64: Geldart, D. Types of gas fluidization. *Powder Technol* **7,** 285–292 (1973).

65: Carrigy, M. A. Experiments on the angles of repose of granular materials. *Sedimentology* **14,** 147-158 (1970).

66: Rowley, P. J., Kokelaar, P., Menzies, M. & Waltham, D. Shear-derived mixing in dense granular flows. *J. Sediment. Res.* **81,** 874-884 (2011).

67: Fielding, C. R. Upper flow regime sheets, lenses and scour fills: Extending the range of architectural elements for fluvial sediment bodies. *Sediment. Geol.* **190,** 227-240 (2006).

ACKNOWLEDGEMENTS

This work was carried out as part of a PhD project funded by a University of Hull PhD scholarship in the Catastrophic Flows Research Cluster. Experiments were performed in the Geohazards Lab at the University of Portsmouth, using equipment funded by a British Society for Geomorphology Early Career Researcher Grant held by PR.

AUTHOR CONTRIBUTIONS

GS carried out experimental work and drafted manuscript. GS, PR, GG, MT, and AS carried out fieldwork. GS, PR, and RW analysed experimental data. GS, PR, RW, GG, MT, AS, and DP discussed results and edited/commented on the manuscript. Characterisation of the experimental materials was led by SC.

COMPETING INTERESTS

The authors declare no competing interests.

FIGURES & CAPTIONS

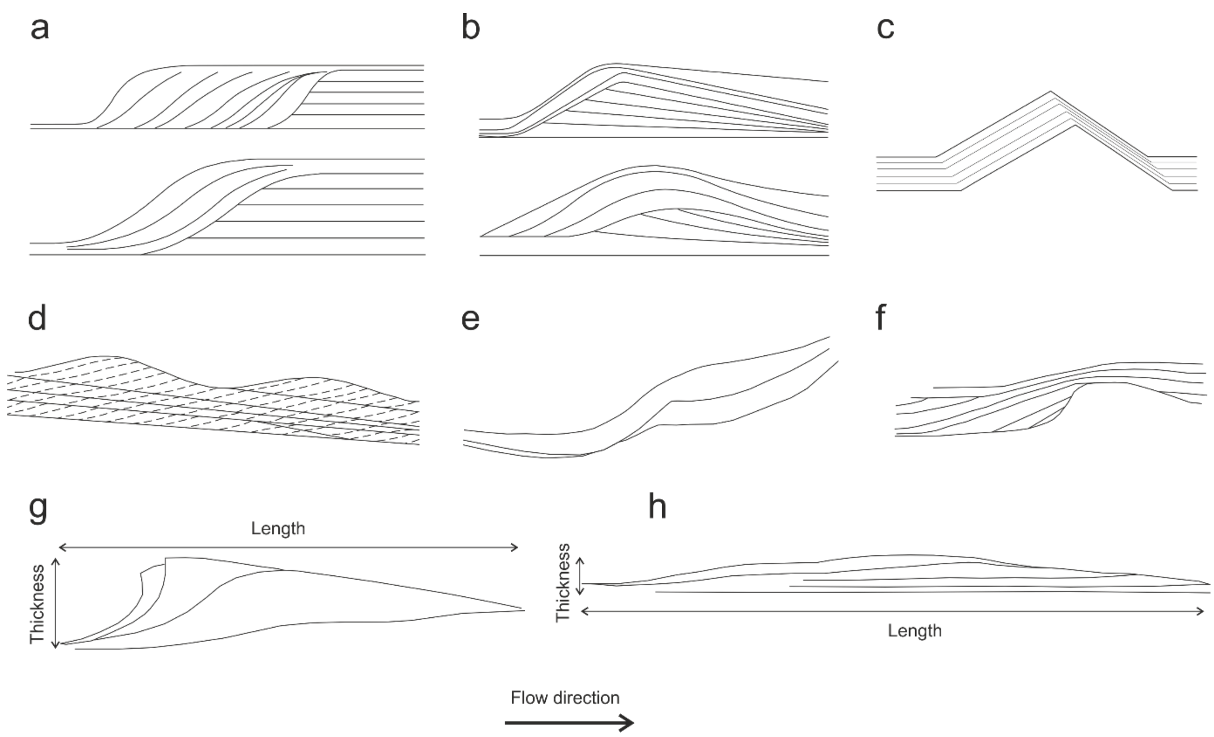

Fig. 1. Examples of dune bedforms deposited by various flow types. **a** Idealised chute-and-pool structures in dilute PDC deposits at Laacher See[33]. **b** Idealised antidunes in dilute PDC deposits at Laacher See[33]. **c** Idealised regressive dune bedform[35]. **d** Idealised stable antidunes[41]. **e** Regressive dune bedform from the Proximal Bedded Deposits at Mt St Helens[46]. **f** Idealised fluvial chute-and-pool structure[67]. **g** Steep stoss side regressive dune

bedform as described in this paper, showing length and thickness definitions. **h** Shallow stoss side dune bedform as described in this paper.

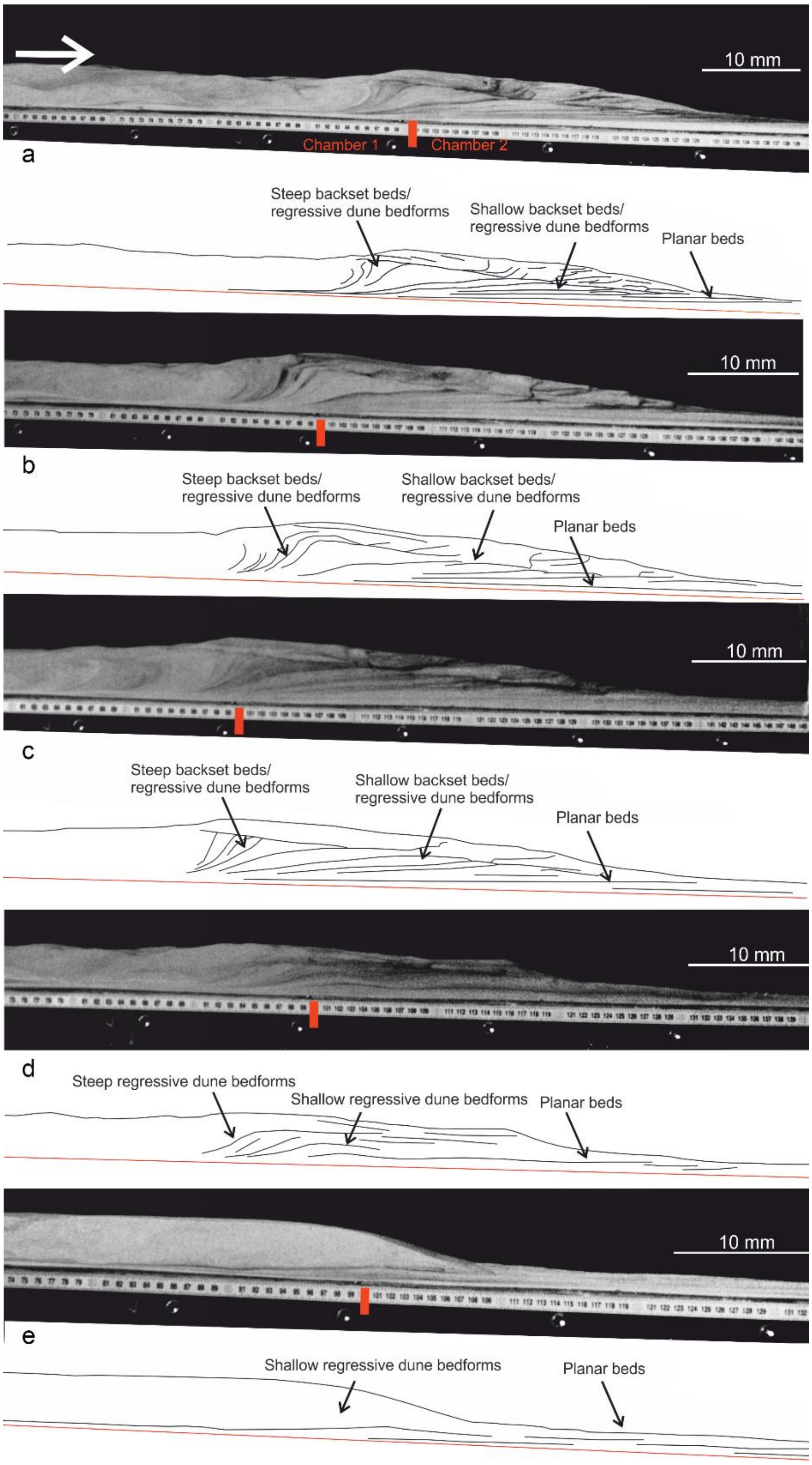

Fig. 2. Deposits from five separate experimental runs. **a**, **b**, **c** show dune bedforms deposited by currents passing above a chamber aerated at 0.93 U_{mf} to one unaerated. **d** shows dune

bedforms deposited by a current passing above a chamber aerated at 0.93 U_{mf} to one aerated at 0.66 U_{mf}. **e** shows dune bedforms deposited by a current passing above a chamber aerated at 0.66 U_{mf} to one aerated at 0.53 $U_{mf.}$

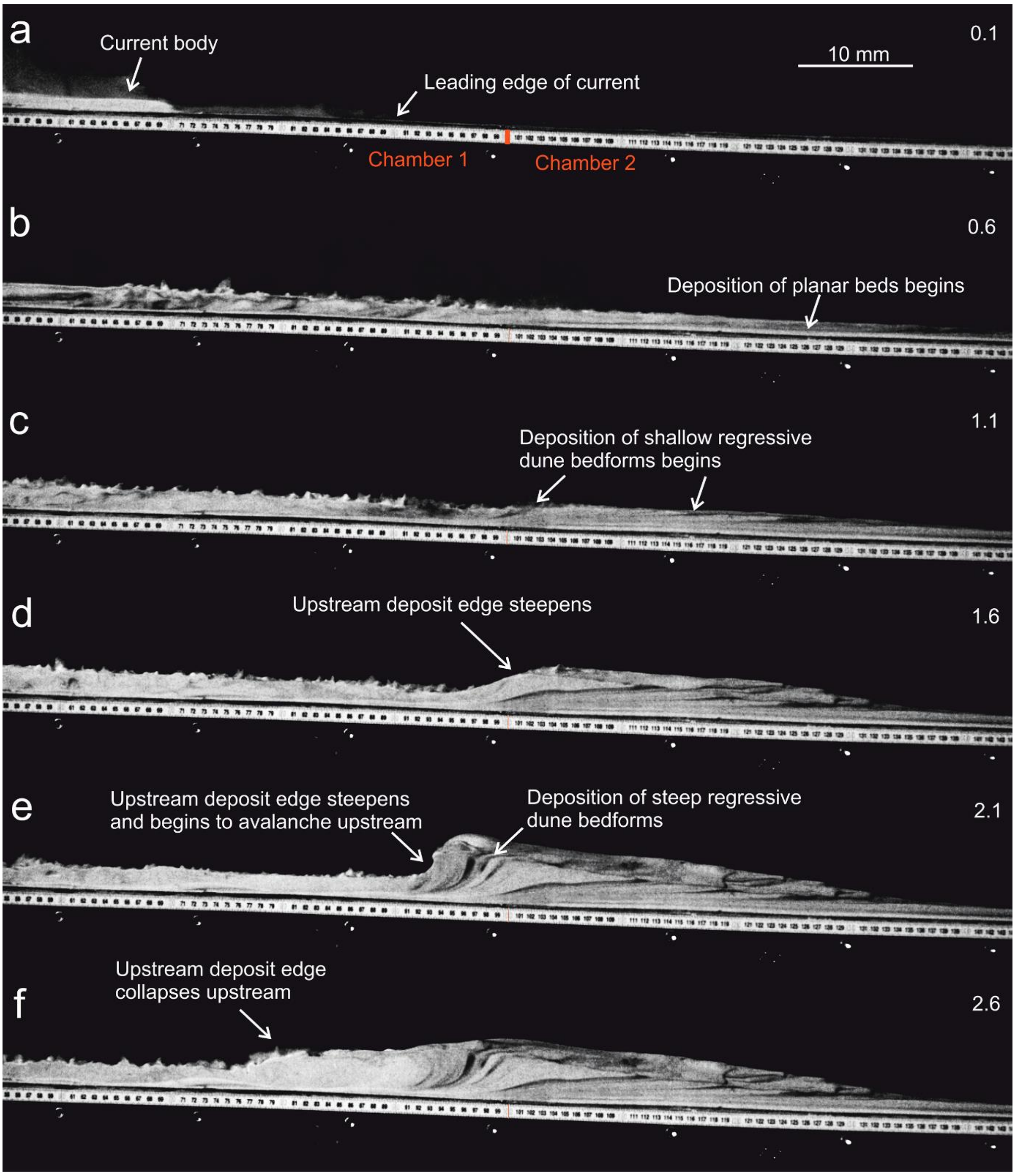

Fig. 3. Timelapse of an experimental granular current. Deposition of dune bedforms is triggered by the current passing above a chamber aerated at 0.93 U_{mf} to one unaerated.

Number in the top right of the frames is the time in seconds since the current entered the first frame.

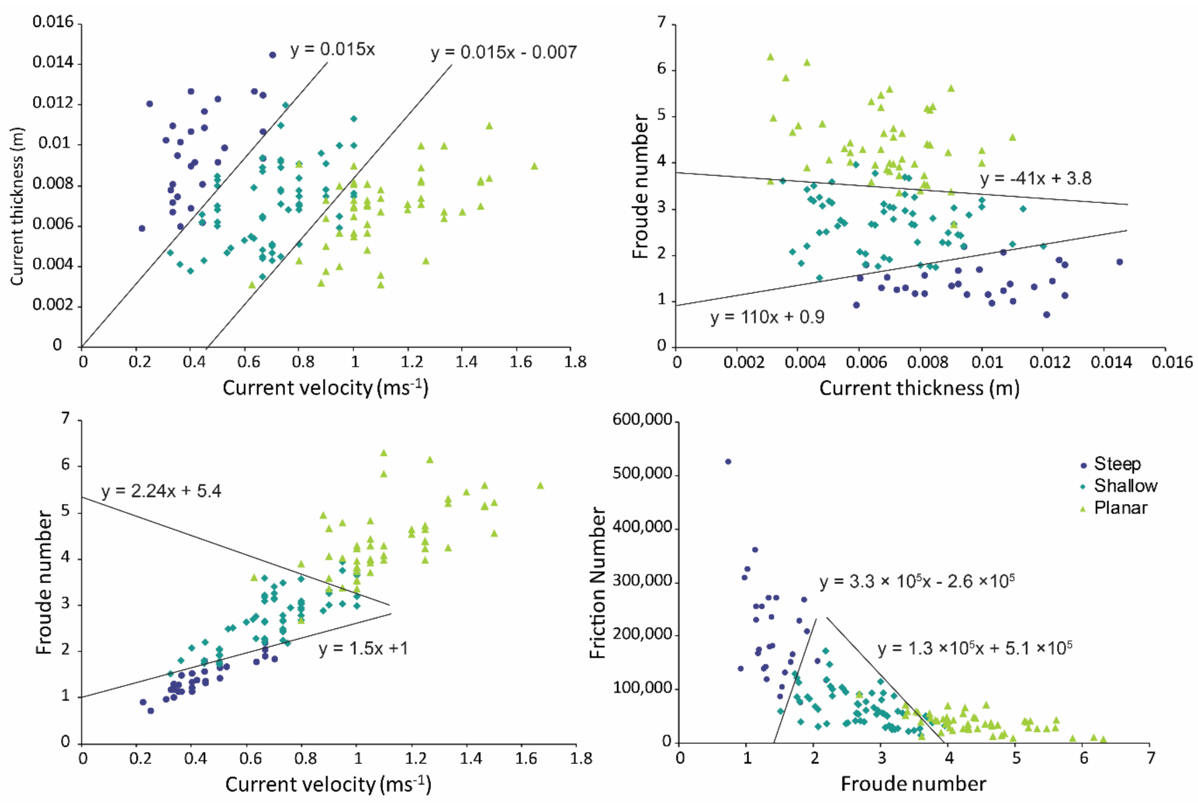

Fig. 4. Phase diagrams showing the current conditions which control dune bedform formation, with plausible phase boundaries. **a** Velocity vs. thickness. **b** Velocity vs. Froude number. **c** Thickness vs. Froude number. **d** Friction number vs. Froude number. Representative (n = 20) error bars are located in the bottom right of each image (± 2σ).

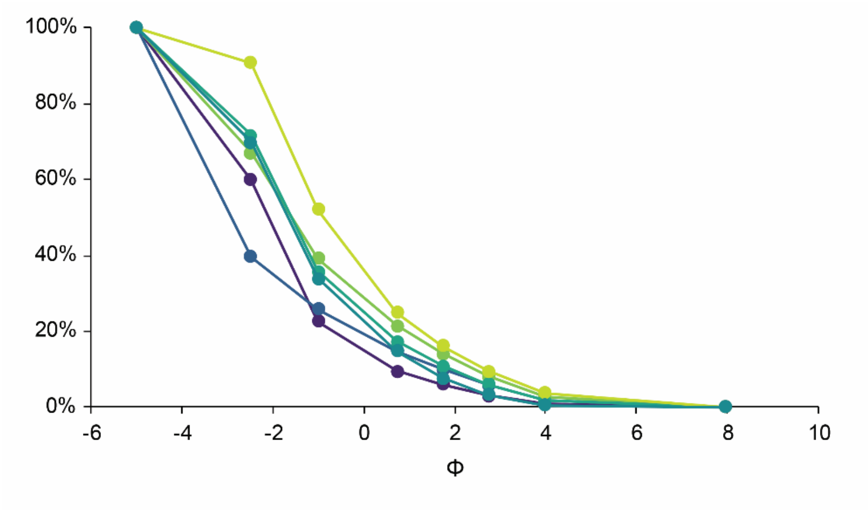

Fig. 5. Grain size distribution curves for six samples from the Pozzolane Rosse ignimbrite. Note the domination by coarse grains and depletion in the <63 μm (4 ϕ) fraction.

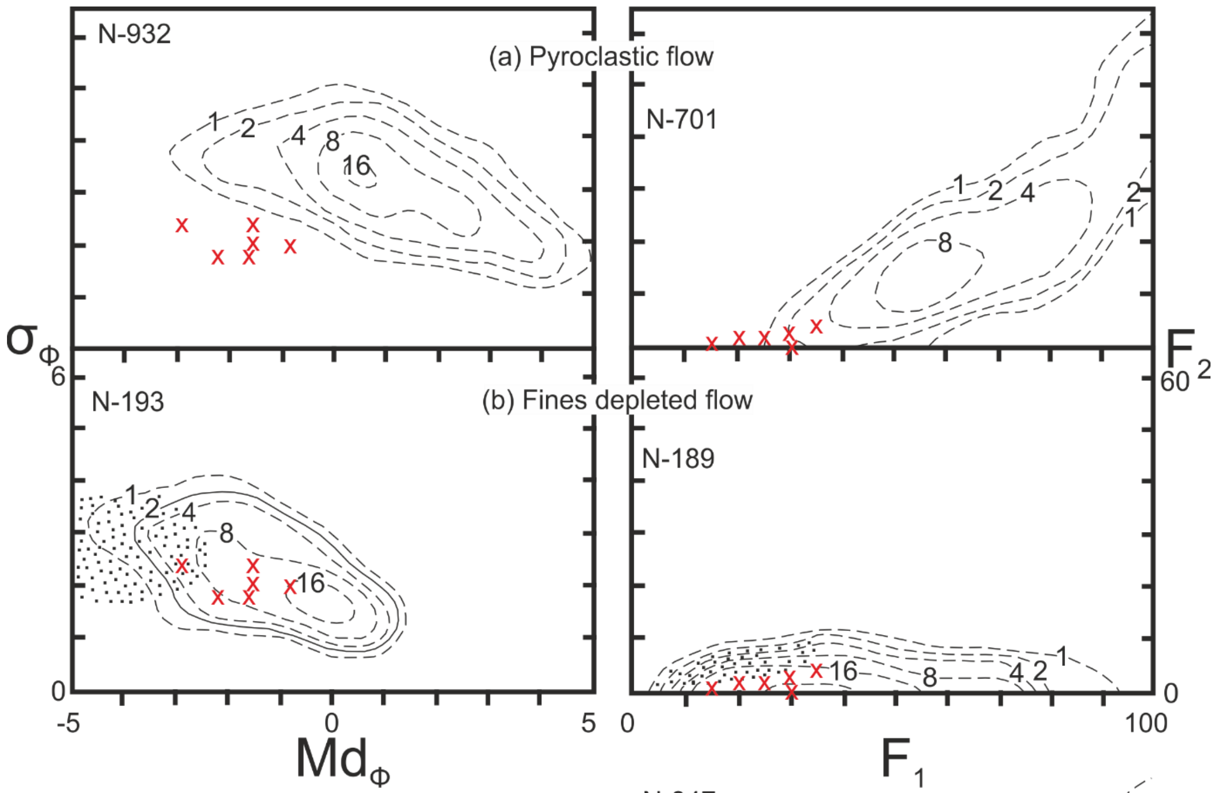

Fig. 6. Plots of Mdφ/σφ and of weight percentage finer than 63 μm (F_2) versus weight percentage finer than 1 mm (F_1), after Walker[35]. **b** includes deposits such as ground layers, fine-depleted ignimbrites, and gas elutriation pipes. Dotted area contains lithic lag breccias.

Red crosses show the position of the Pozzolane Rosse ignimbrite samples. See also Giordano and Dobran[59].

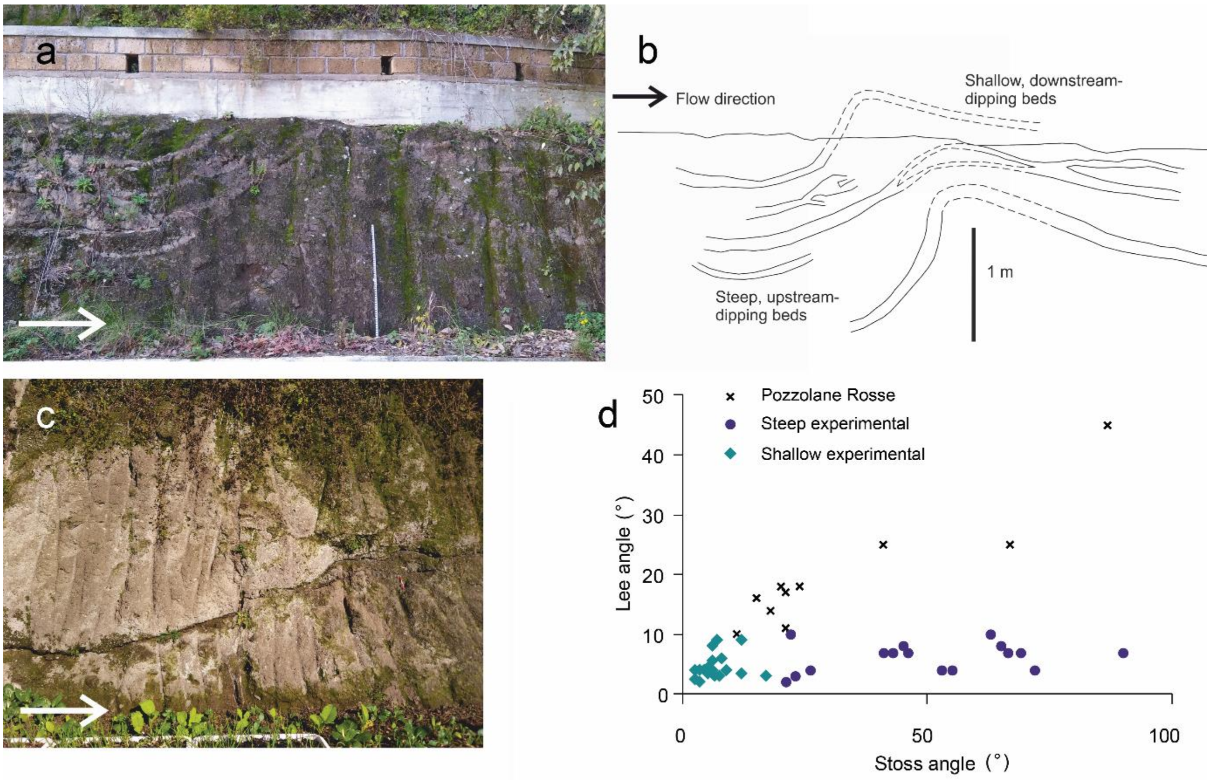

Fig. 7. Field photos and data of the Pozzolane Rosse ignimbrite erupted from Colli Albani, Italy. Flow direction left to right. Coordinates are for UTM 33T grid. **a** steep stoss side dune bedform at 322848 4639168 (ruler 1 m) **b** annotated sketch of the bedform showing the difference in angle between the stoss and lee beds **c** shallow stoss side dune bedform at 333920 4623281 (pen below crest is 0.15 m) **d** shows that several of these dune bedforms have similar stoss angles to our experimental features, however the lee angles are much steeper.

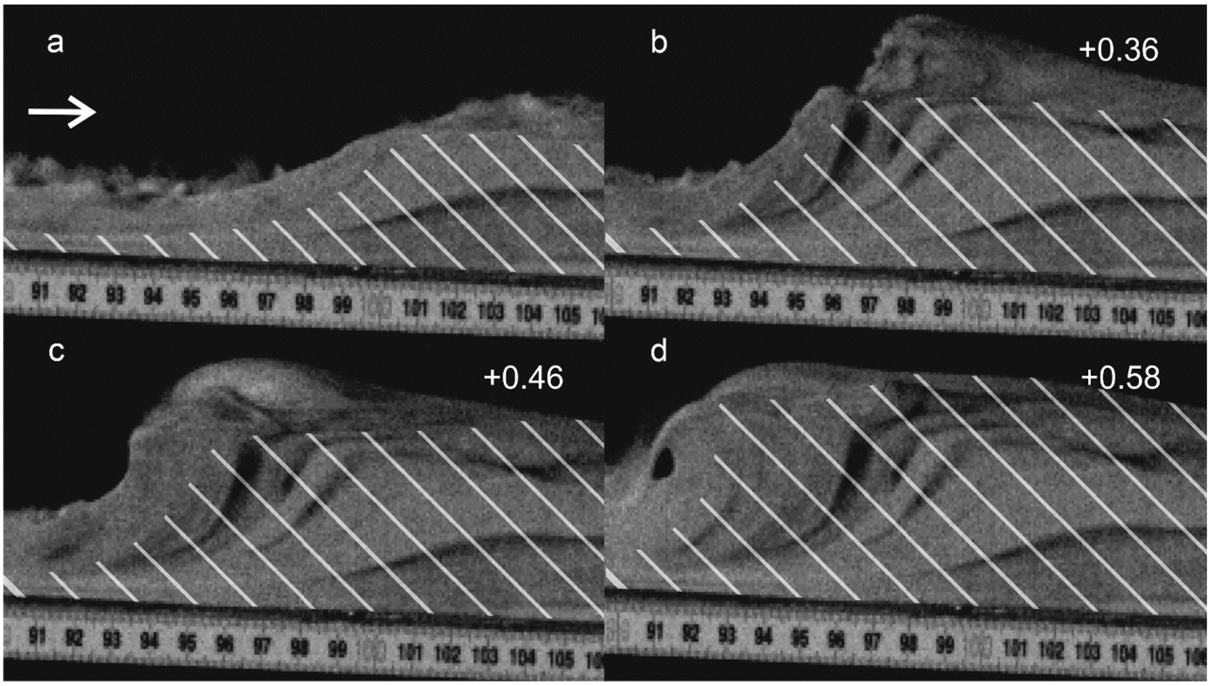

Fig. 8. The formation and evolution of a granular jump. Numbers in the top right are seconds passed since the first frame. Shaded area shows stationary deposit. Flow direction left to right. **a** shows the initial formation of a steepening bump. **b** shows the upstream migration and further steepening of the jump, which has two separate fronts separated by a shelf. **c** The upper front has collapsed, and the lower front is vertical. **d** The lower front of the jump collapses upstream by avalanching.

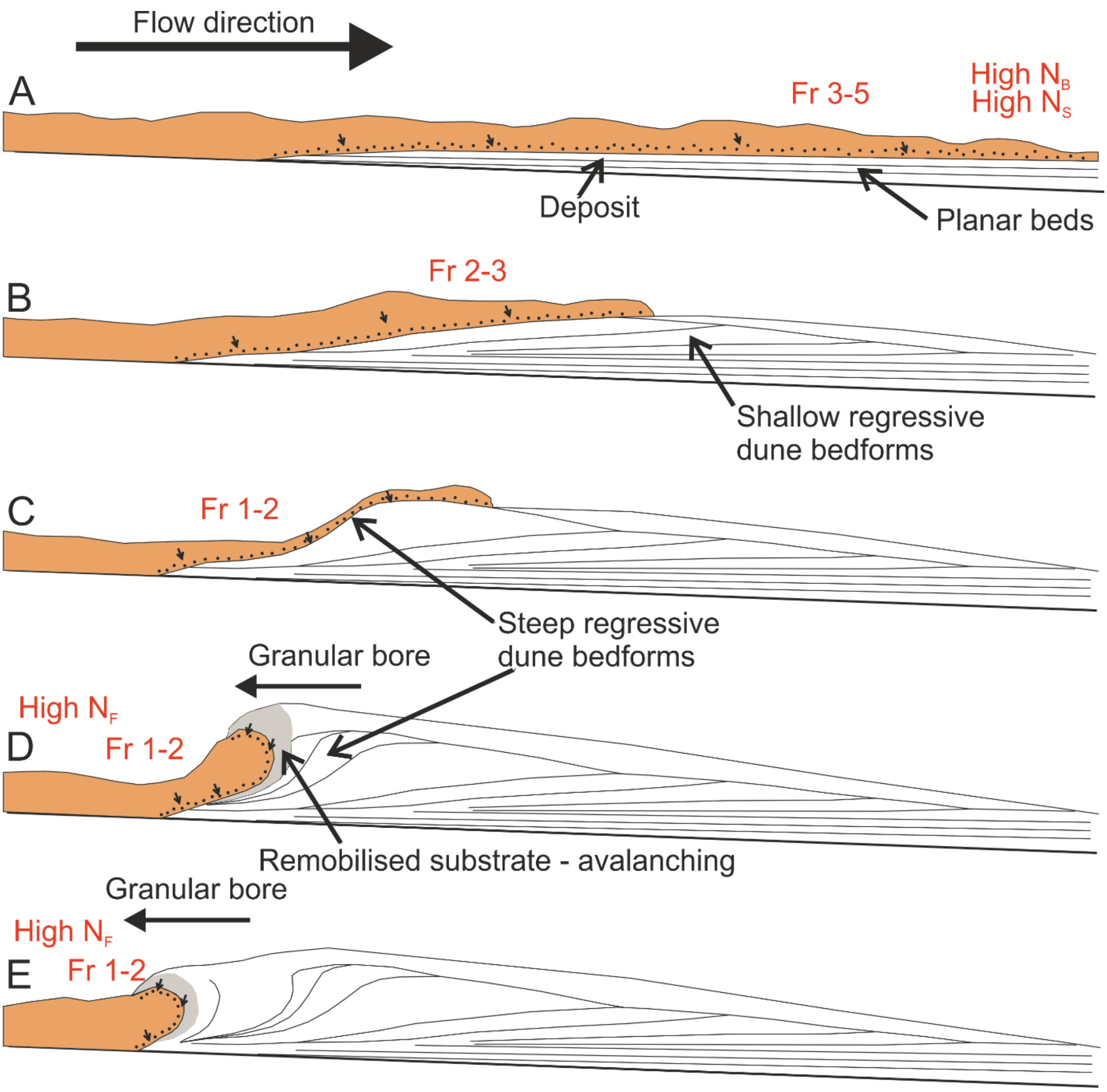

Fig. 9. Schematic showing how different dune bedforms could be deposited by a PDC. Flow properties in red (Fr, N_S, N_B, N_F) refer to the Froude, Savage, Bagnold, and Friction Numbers respectively.

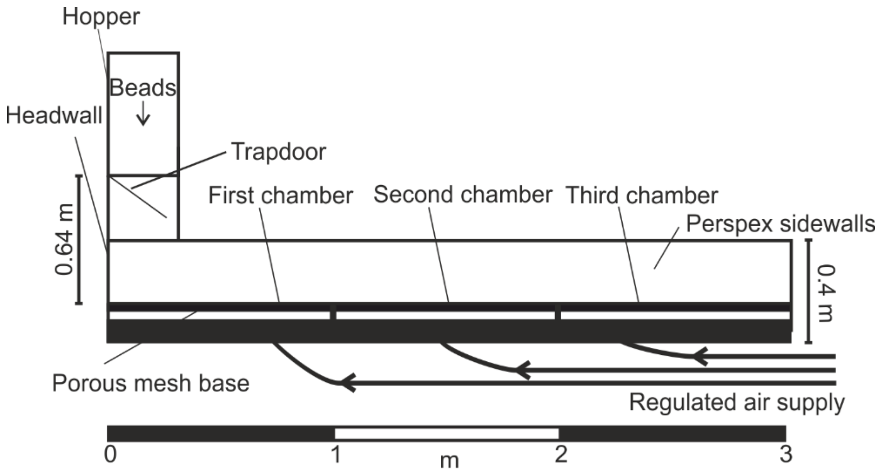

Fig. 10. A longitudinal section view of the experimental flume.